# Supporting Information for

# Efficient harvest of electricity, aromatic aldehydes and $H_2$ from lignin over nanoflower-like cobalt-based bifunctional electrocatalysts

**Yichen Zhang [1,2] ‡, Daihong Gao[1,2] ‡, Denghao Ouyang [1,2], Binhang Yan [2], Xuebing Zhao [1,2] ***

[1] Key Laboratory of Industrial Biocatalysis, Ministry of Education; Tsinghua University, Beijing 100084, China;

[2] Department of Chemical Engineering, Tsinghua University, Beijing 100084, China.

‡These authors contributed equally to this work.

* Corresponding author: Xuebing Zhao. Email: zhaoxb@mail.tsinghua.edu.cn

**Fig. S1** Effect of electrodeposition conditions on the electrochemical performance (LSV curve) of $CoS_x$@NF electrode for lignin electro-oxidation. **(a)** Effects of electrodeposition time; **(b)** Effects of electrodeposition current density

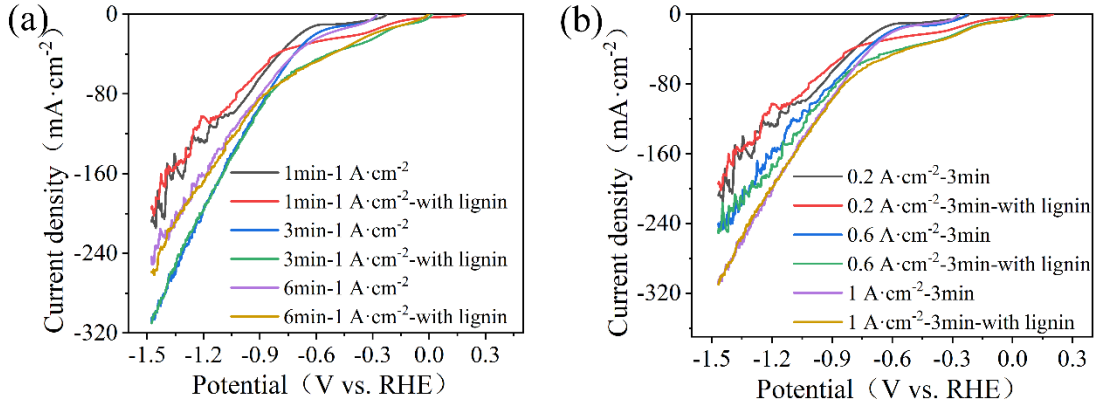

**Fig. S2** SEM images of $CoS_x$@NF electrodes prepared at different deposition time: (**a)-(c)** electrodeposition for 1 min; (**d)-(f)** electrodeposition for 3 min; (**g)-(i)** electrodeposition for 6 min; reaction conditions: electrodeposition current was 1 A $cm^{-2}$

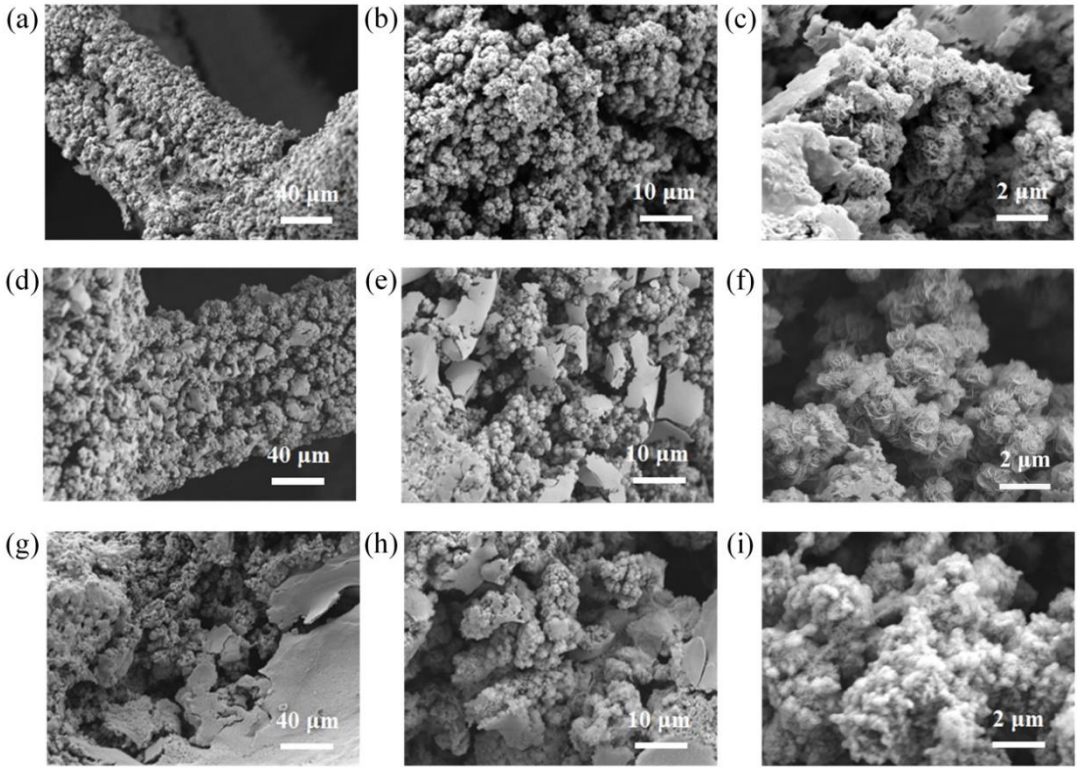

**Fig. S3** SEM images of $CoS_x$@NF electrodes prepared at different deposition current densities: **(a)-(c)** 0.2 A $cm^{-2}$; **(d)-(f)** 0.6 A $cm^{-2}$; reaction conditions: deposition time was 3 min

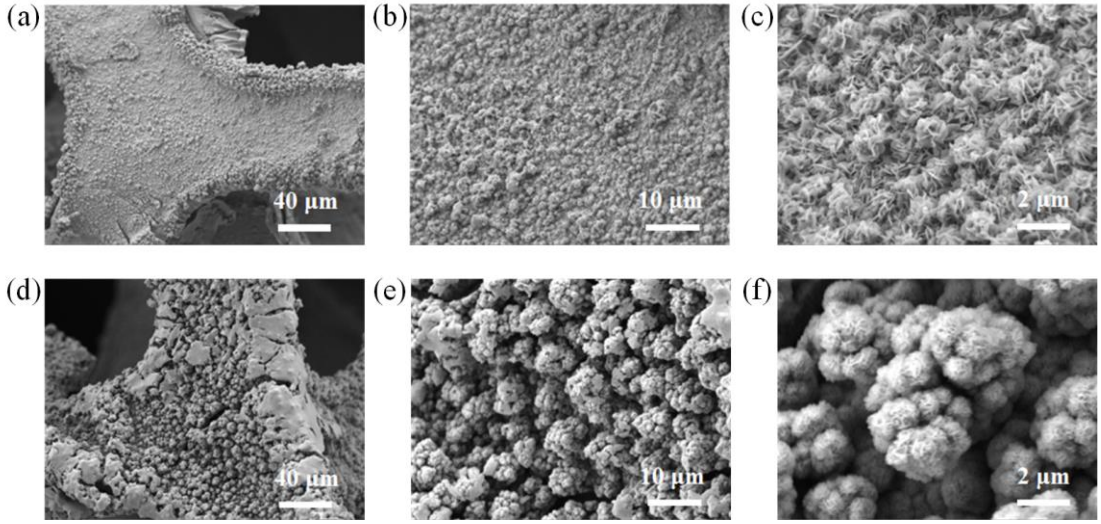

**Fig. S4** XPS spectra of Ni 2p **(a)** and S 2p **(b)** of $CoS_x$@NF

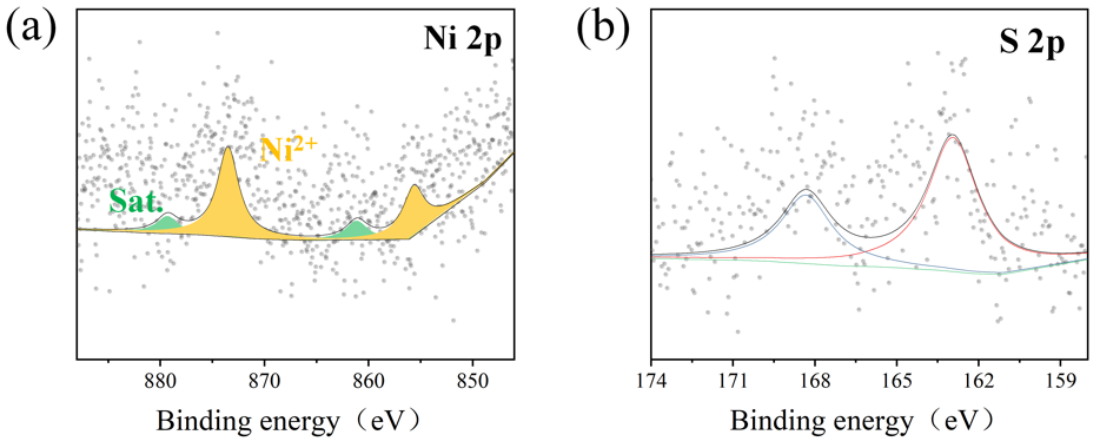

**Fig. S5** BET specific surface area of different electrodes: $CoS_x$@NF was prepared by electrodeposition at a current density of 1 A $cm^{-2}$; lc-$CoS_x$@NF was prepared by electrodeposition at a current density of 3.2 mA $cm^{-2}$; NF is raw nickel foam.

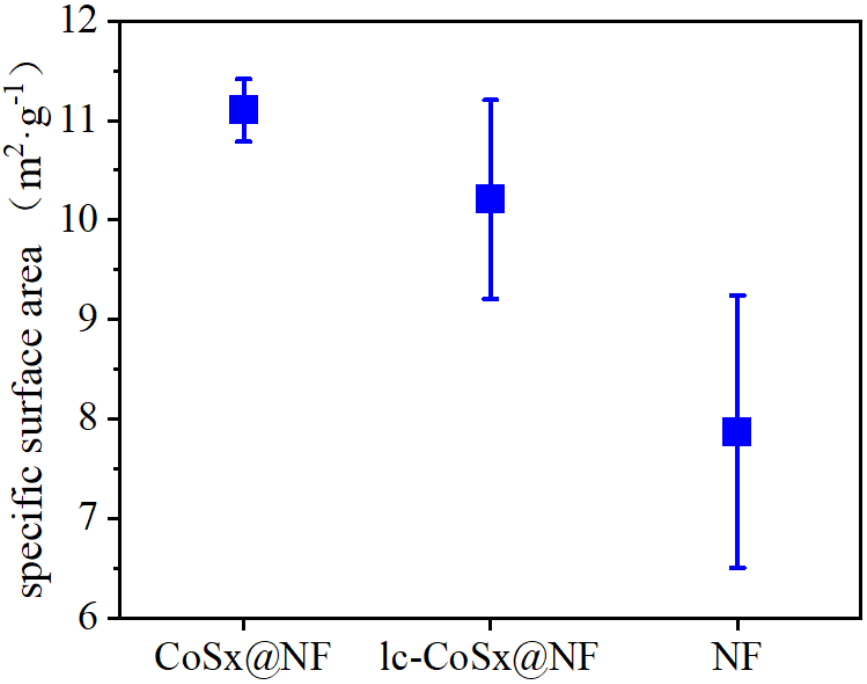

**Fig. S6** CV curves and $C_{dl}$ fitting diagrams of different electrodes: **(a)** NF; **(b)** $CoS_x$@NF; **(c)** lc-$CoS_x$@NF; **(d)** $C_{dl}$ fitting value

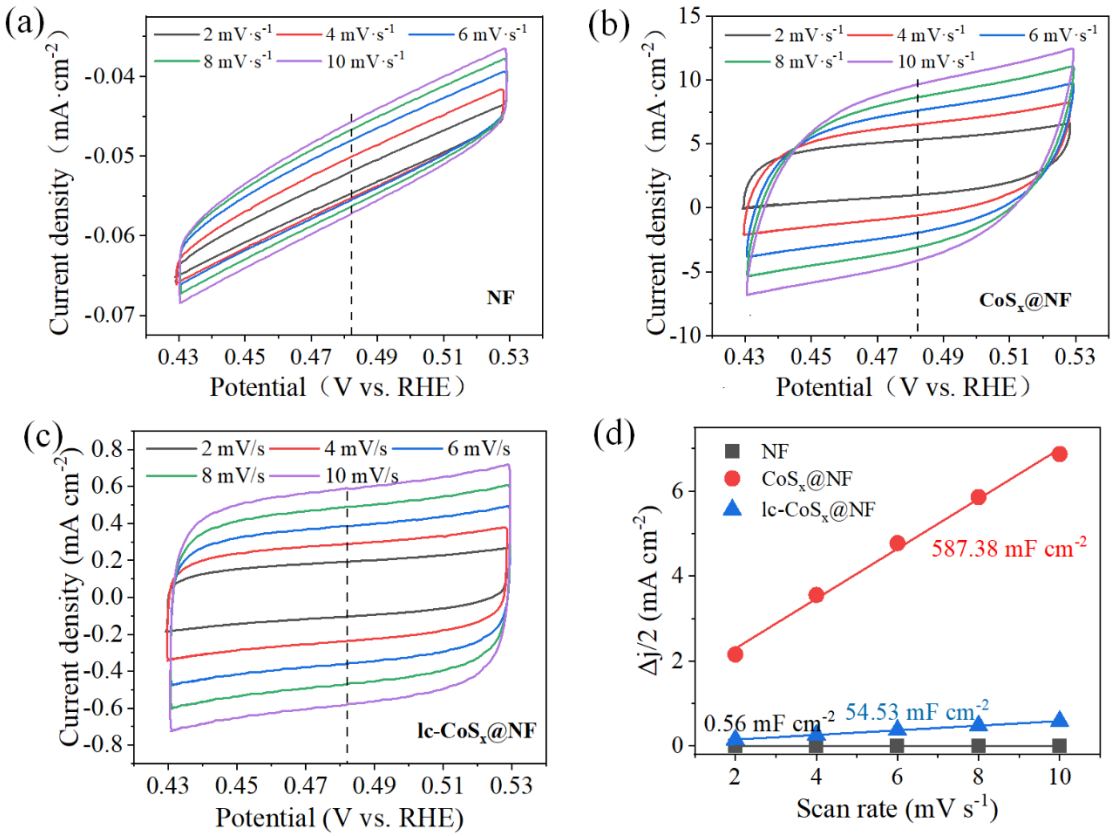

**Fig. S7** Nyquist curves of different anodes: (**a**) full image; (**b**) high-frequency region magnification.

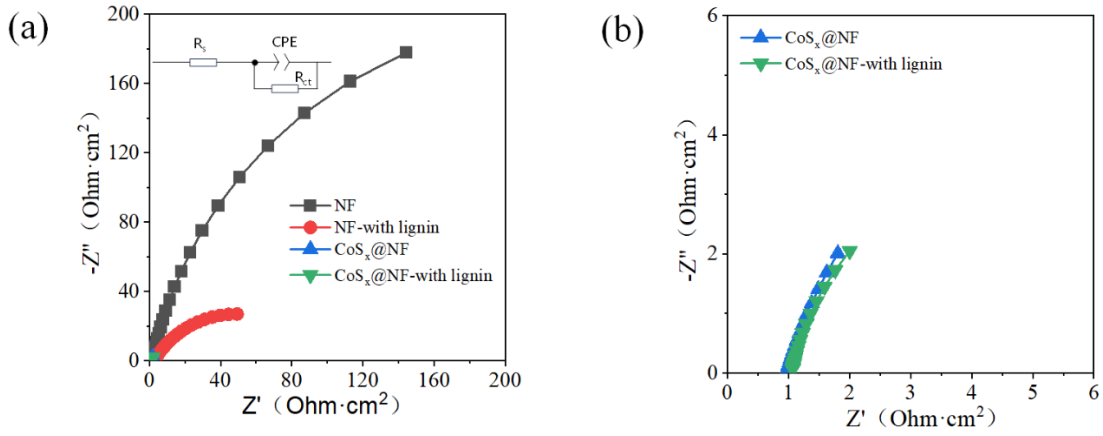

**Fig. S8** Effect of alkali concentration on the yield of aromatic aldehydes by electro-oxidative depolymerization of lignin: (**a**) *p*-hydroxybenzaldehyde; (**b**) vanillin; (**c**) syringaldehyde; (**d**) total aromatic aldehydes; reaction conditions: $C_{lignin}$, 2 g $L^{-1}$; $V_{electrolysis}$, 1.2 V; $T$, 80 ℃; $A$, 2×2 $cm^2$ electrode area

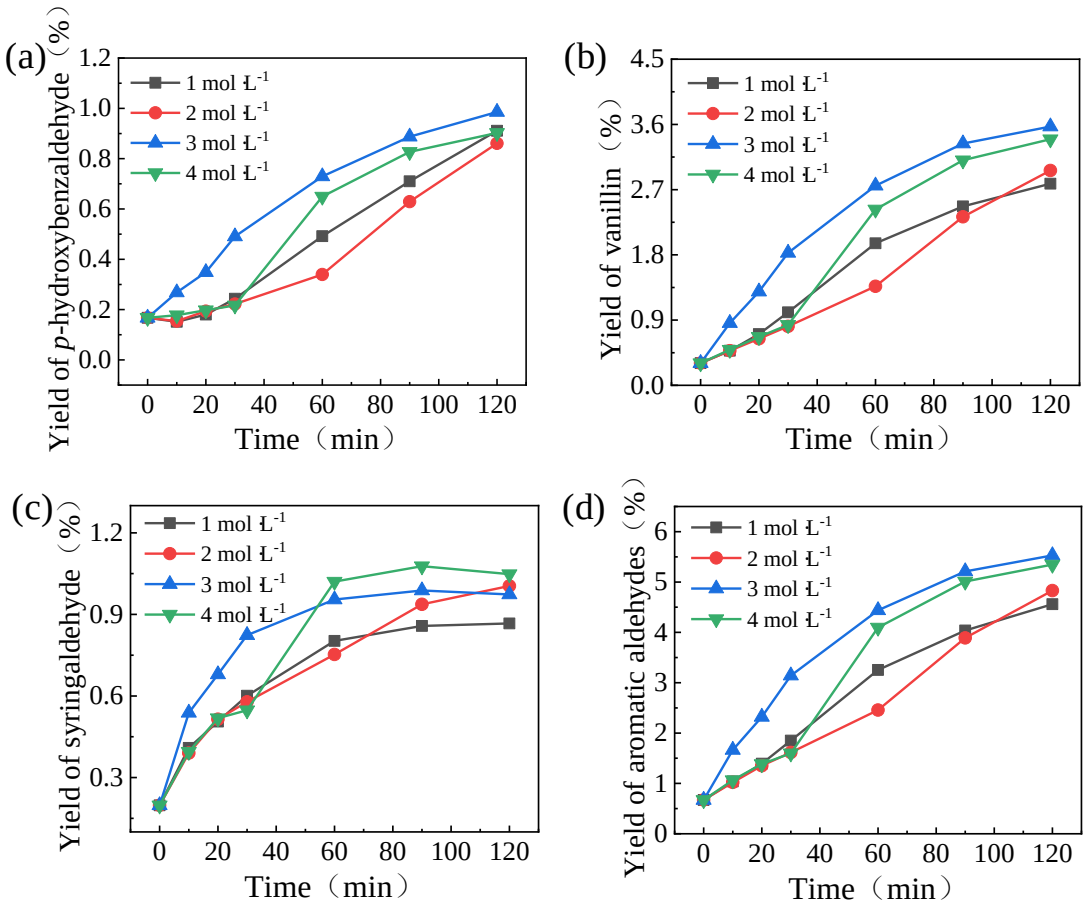

**Fig. S9** Effects of lignin concentration on the yield of aromatic aldehydes by lignin depolymerization: (**a**) *p*-hydroxybenzaldehyde; (**b**) vanillin; (**c**) syringaldehyde; (**d**) total aromatic aldehydes; reaction conditions: $V_{electrolysis}$, 1.2 V; $C_{KOH}$, 3 mol $L^{-1}$; *T*, 80 ℃; *A*, 2×2 $cm^2$ electrode area

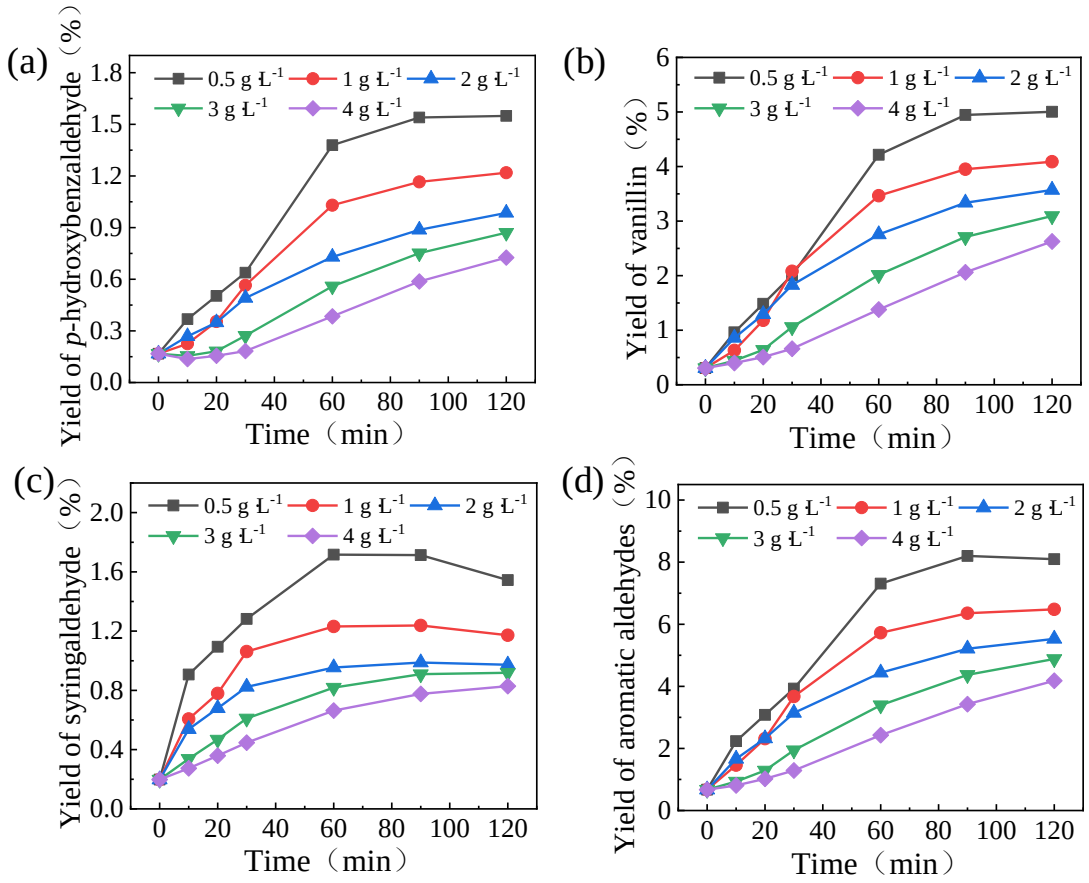

**Fig. S10** Effects of temperature on the yield of aromatic aldehydes by electro-oxidative depolymerization of lignin: **(a)** *p*-hydroxybenzaldehyde; **(b)** vanillin; **(c)** syringaldehyde; **(d)** total aromatic aldehydes; reaction conditions: $C_{lignin}$, 2 g $L^{-1}$; $C_{KOH}$, 3 mol $L^{-1}$; $V_{electrolysis}$, 1.2 V; $A$, 2×2 $cm^2$ electrode area

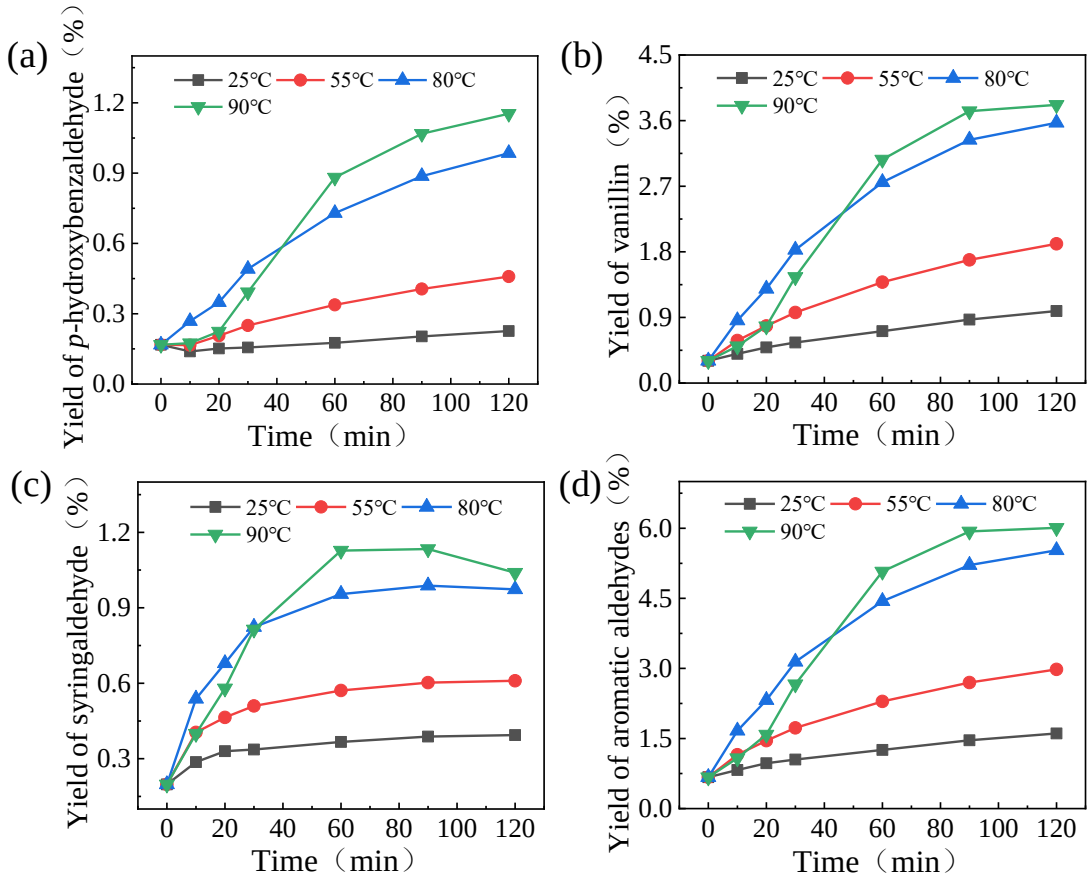

**Fig. S11** Structural characterization of used $CoS_x$@NF anode: **a-c** SEM images; **d-f** XPS spectra of Co 2p **d**, Ni 2p **e**, and S 2 p **f**; **g** XRD spectra of $CoS_x$@NF (red line), Ni (blue line), and CoOOH (red line)

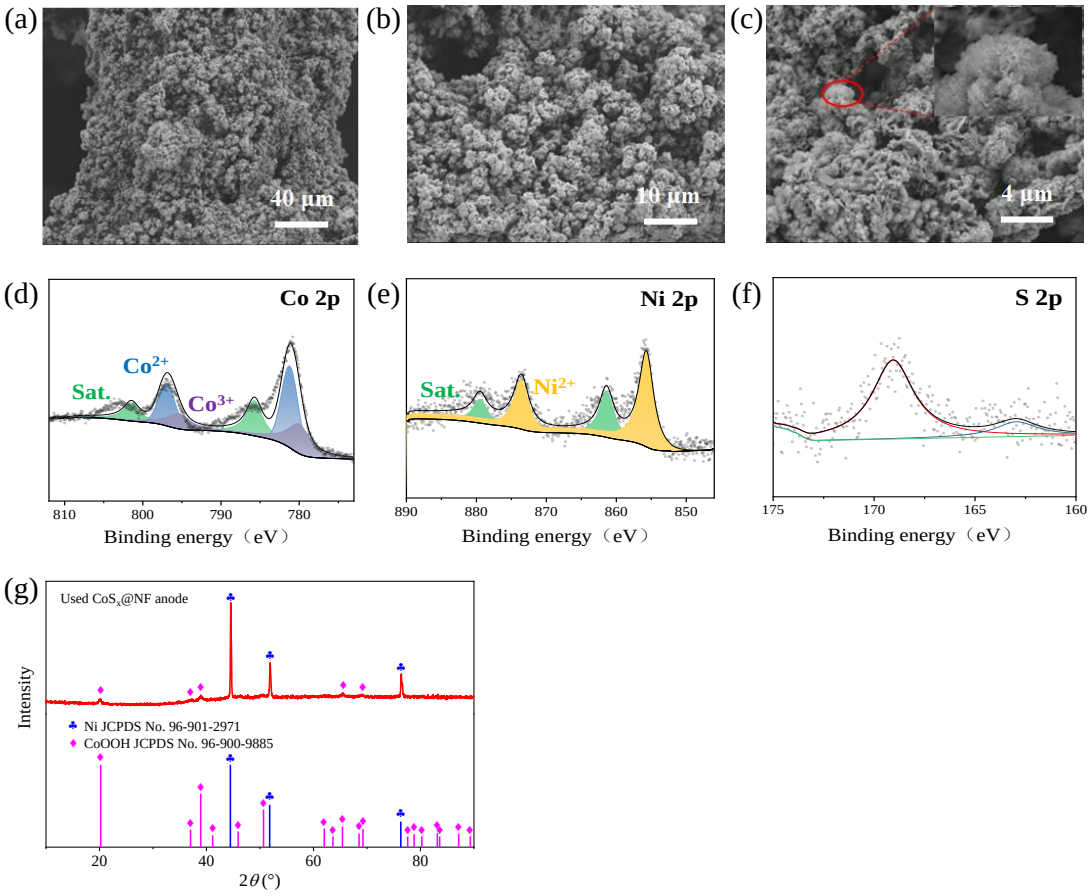

**Fig. S12** Effect of electrodeposition conditions on the hydrogen evolution performance of $CoS_x$@NF electrode: **(a)** deposition time; **(b)** deposition current density

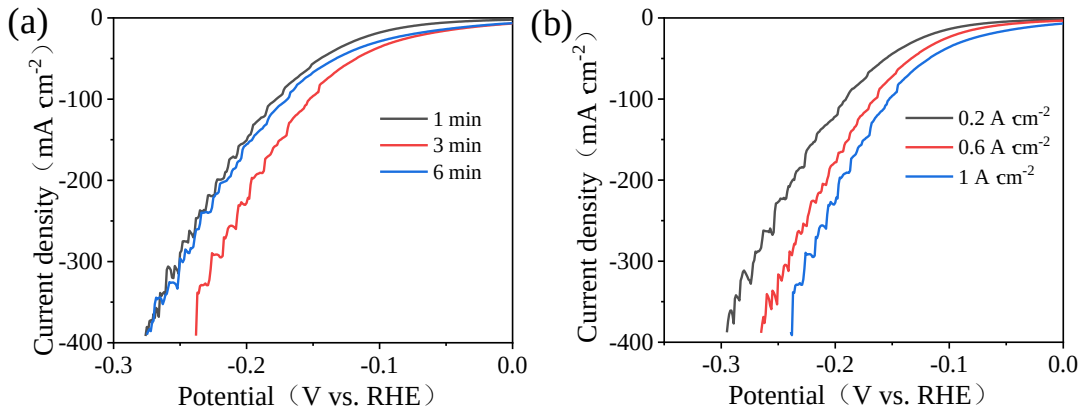

**Fig. S13** Nyquist curves of different cathodes: (**a)** full image at the hydrogen evolution overpotential of 113 mV; (**b)** Nyquist curves at different hydrogen evolution overpotentials; (**c)** equivalent circuit diagram

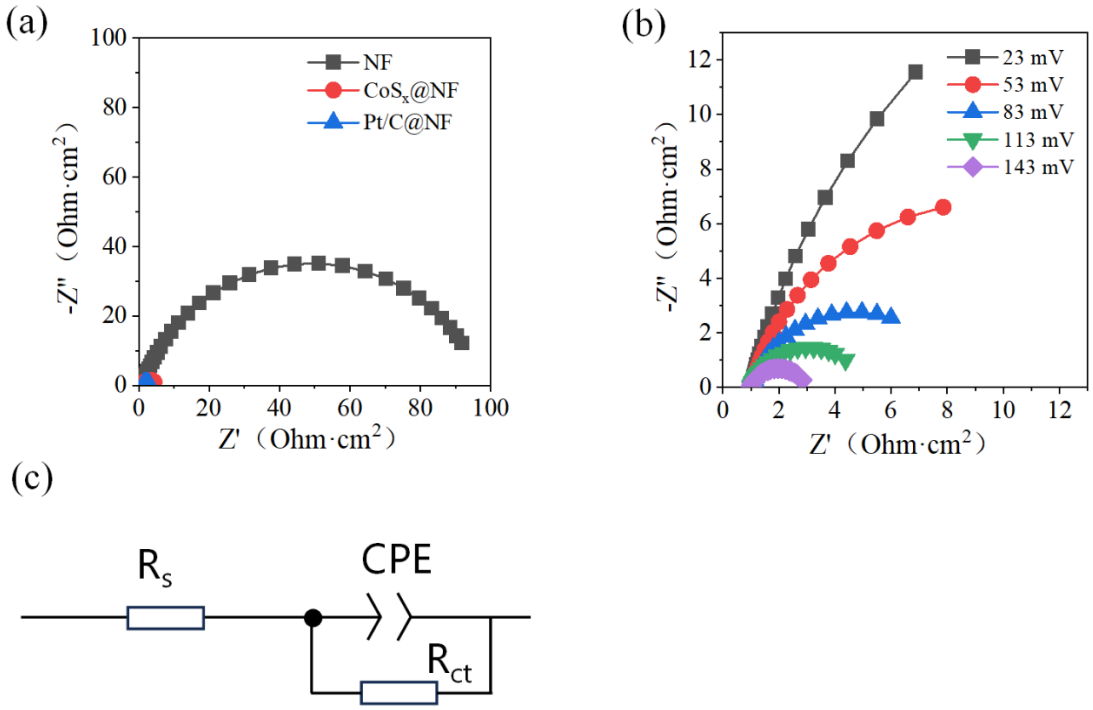

**Fig. S14** Structural characterization of used $CoS_x$@NF cathode: (**a)-(c)** SEM images; (**d)-(f)** XPS spectra of Co 2p, Ni 2p, and S 2 p; (**g**) XRD spectra of $CoS_x$@NF (red line) and Ni (blue line) after use

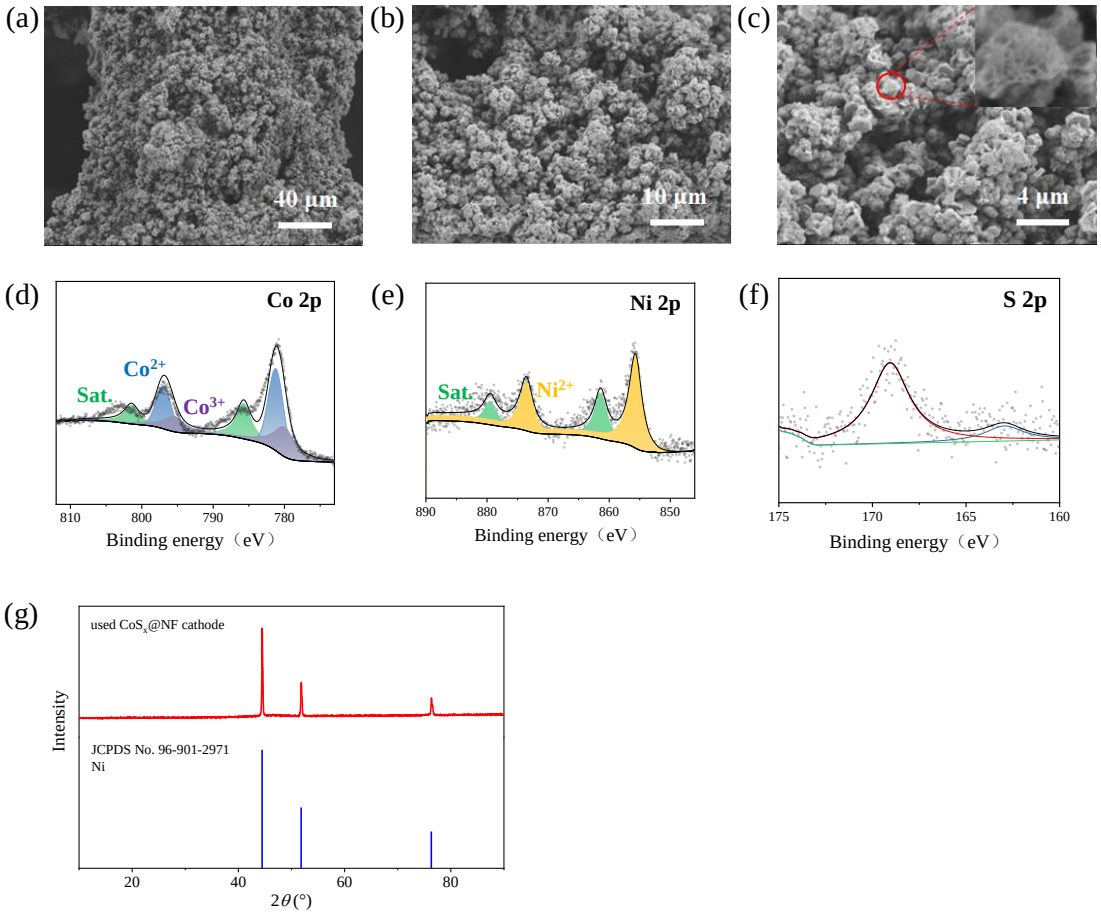

**Fig. S15** Catalyst models used in density functional theory calculations: Top view (**a)** and side view (**b)** of $CoS_2$ (010); top view (**c)** and side view (**d)** of $CoS_2$ (111); top view (**e)** and side view (**f)** of Ni (111); top view (**g)** and side view (**h)** of Pt (111).

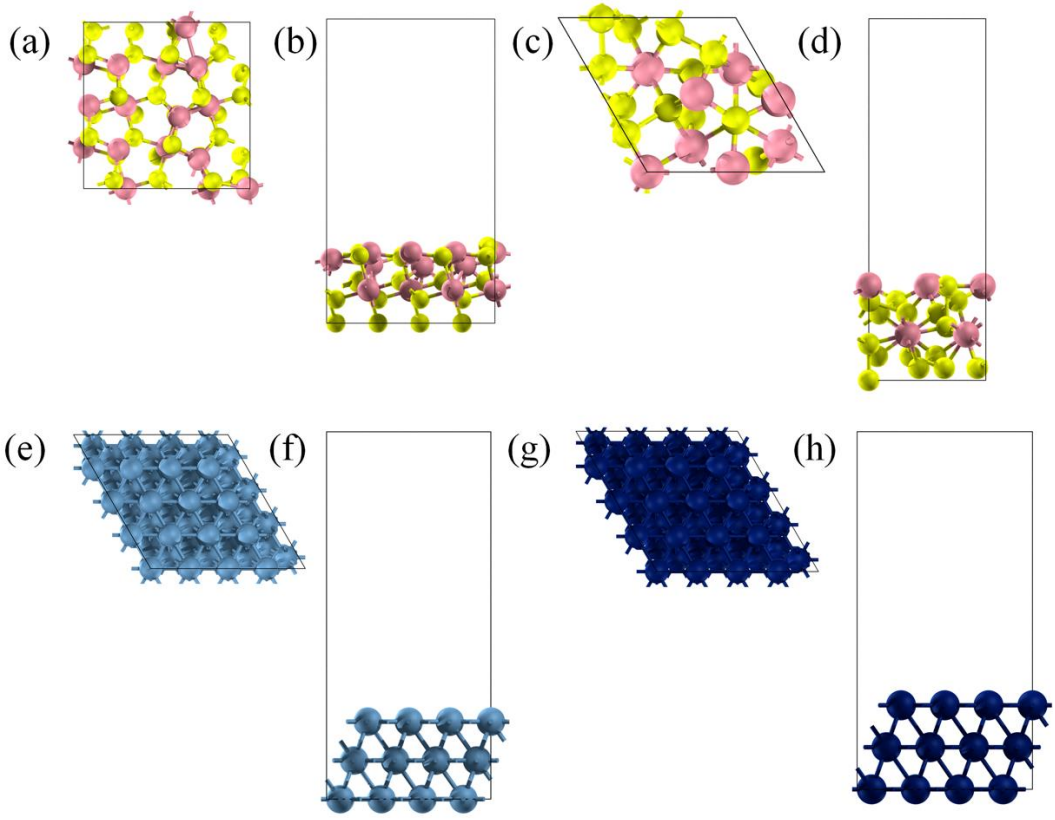

**Fig. S16** Voltage and current relationship between the DLFC Output and electrolytic cell input for lignin depolymerization and hydrogen Evolution

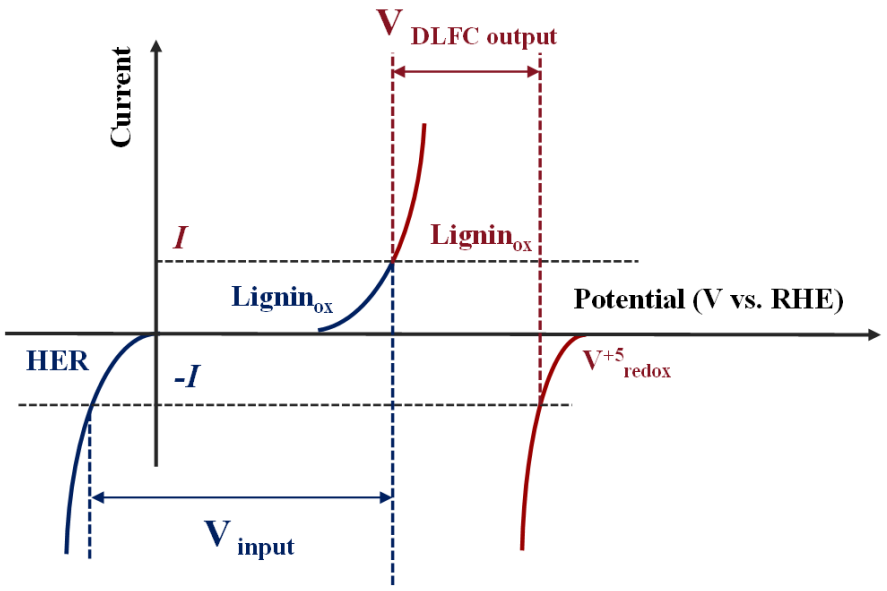

**Fig. S17** Current/voltage-time curves of the coupled system and comparison with the constant voltage electrolysis system

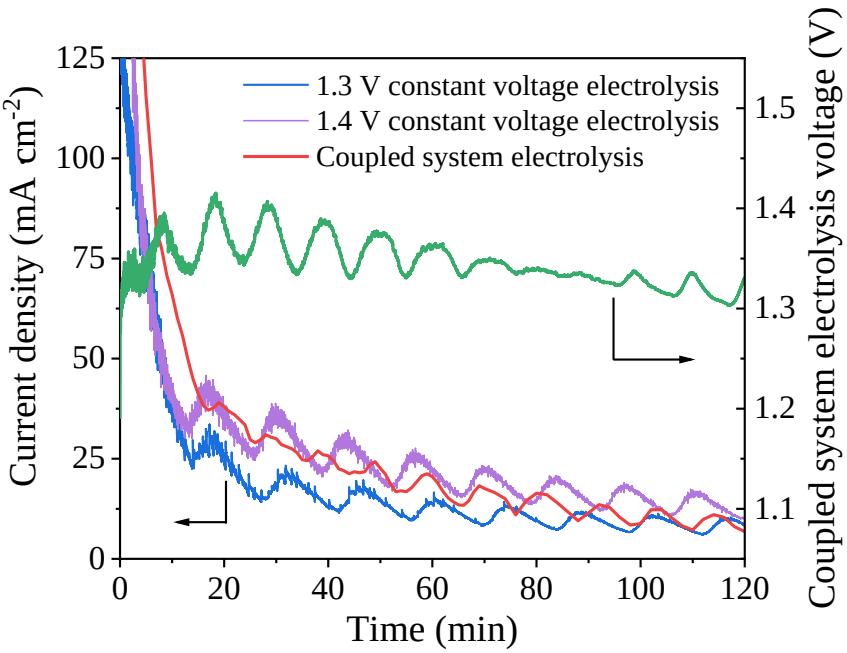

**Table S1** Some studies related to the electrooxidative depolymerization of lignin reported in recent years

| Raw material | Elehctrode | Electrolyte | Initial lignin conc. | Current | Time | Temp. | Main product yield | Ref. |
|---|---|---|---|---|---|---|---|---|
| Spruce lignosulfonate | Nickel mesh | 3 mol $L^{-1}$ NaOH | 1.04% w/v | 6.1 mA $cm^{-2}$ | 2.5 h | 170 ℃ | 9.6% vanillin | [1] |
| Wheat straw alkali lignin | SS-304 | 1 mol $L^{-1}$ NaOH | 10 g $L^{-1}$ | 50 mA $cm^{-2}$ | 16 h | RT | 6% vanillin | [2] |
| Corn stover lignin | $Pb/PbO_2$ | 1 mol $L^{-1}$ NaOH | 50 g $L^{-1}$ | 25 mA $cm^{-2}$ | 1 h | 40 ℃ | 2.24% ferulic acid, 1.11% vanillin, 0.24% acetovanillone, 1.00% syringaldehyde | [3] |
| Kraft lignin | Activated Foam | 3 mol $L^{-1}$ NaOH | 5 g $L^{-1}$ | 38 mA $cm^{-2}$ | 2688 C $g^{-1}$ | 80 ℃ | 1.8% vanillin | [4] |
| Indulin AT lignin | Nickel | 3 mol $L^{-1}$ NaOH | 0.6%wt | 10 mA $cm^{-2}$ | 2700 C $g^{-1}$ | 160 ℃ | 1.8% vanillin, 1.1% acetovanillone | [5] |
| Wheat straw and sakanda grass lignin | Nickel wire | 1 mol $L^{-1}$ NaOH | 20 g $L^{-1}$ | 0.4 V vs. Ag/AgCl | 4 h | RT | 0.12% vanillin, 0.12% vanillin aldehyde, 0.15% vanillin ethyl ketone, 0.32% erucic acid | [6] |
| Lignin | DS-Co@Carbon paper | 1 mol $L^{-1}$ NaOH | 10 g $L^{-1}$ | 1.05 V vs. RHE | 25 h | NA | 2.4% *p*-hydroxybenzaldehyde, 3.8% vanillin, 4.2% eugenaldehyde, 0.9% benzoic acid | [7] |

| | | | | | | | | |
|---|---|---|---|---|---|---|---|---|
| Corn stover alkali lignin | CoS@NF, direct lignin fuel cell for lignin oxidation | 3 M KOH | 0.5 g/L | 0.9 V output voltage | 120 h | 80 °C | 1.43% p-hydroxybenzaldehyde, 5.31% vanillin, 1.06% syringaldehyde | [8] |
| Corn stover alkali lignin | $CoS_x$@NF electrode | 3 M KOH | 0.5 g/L | 1.2 V | 1.5 h | 80 °C | 1.55% *p*-hydroxybenzaldehyde, 5.00% vanillin, 1.54% syringaldehyde | This work |

**Table S2** The yields of main aromatic aldehydes during reuse of the anode (weight %)

| Reuse time | *p*-hydroxybenzaldehyde (%) | Vanillin (%) | Syringaldehyde (%) | Total aromatic aldehydes (%) |
|---|---|---|---|---|
| 1 | 0.91 | 3.27 | 0.92 | 5.11 |
| 2 | 0.85 | 3.39 | 0.92 | 5.16 |
| 3 | 0.89 | 3.53 | 0.96 | 5.38 |
| 4 | 0.92 | 3.65 | 1.01 | 5.58 |
| 5 | 0.93 | 3.68 | 1.03 | 5.64 |

**Table S3** Comparison on the performance of alkaline hydrogen evolution catalysts reported in recent years

| Catalysts/Electrodes | Electrolyte | Overpotential at 10 mA $cm^{-2}$ (mV) | Overpotential at 100 mA $cm^{-2}$(mV) | Tafel slope ($mV\ dec^{-1}$) | Ref. |
|---|---|---|---|---|---|
| $Co_3O_4$@CF (Co foam) | 1 mol $L^{-1}$ KOH | 177 | 294 | — | [9] |
| $CeO_2/Cu_3P$@NF | 1 mol $L^{-1}$ KOH | — | 148 (20 mA $cm^{-2}$) | 132 | [10] |
| Co/$Co_3O_4$@NF | 1 mol $L^{-1}$ KOH | 90 | 129 (20 mA $cm^{-2}$) | 44 | [11] |
| Co/CoP@NF | 1 mol $L^{-1}$ KOH | 35 | 130 | 71 | [12] |
| $MoS_2$/NiS/$MoO_3$@Ti foil | 1 mol $L^{-1}$ KOH | 91 | 157 | 55 | [13] |
| $NiCo_2S_4/Ni_3S_2$@NF | 1 mol $L^{-1}$ KOH | 119 | — | 105.2 | [14] |
| Pt@NF | 1 mol $L^{-1}$ KOH | — | 75 | 120 | [15] |
| Sn/$CoS_2$@CC | 1 mol $L^{-1}$ KOH | 161 | — | 94 | [16] |
| GDY/$CoS_2$@CC | 1 mol $L^{-1}$ KOH | 97 | 318 | 56 | [17] |
| $V_s$-$CoS_2$@CC | 1 mol $L^{-1}$ KOH | 170 | — | 95 | [18] |
| $CoS_x$@NF | 1 mol $L^{-1}$ KOH | 23 | 153 | 136.9 | This work |

## References


1 C. Z. Smith, J. H. P. Utley and J. K. Hammond, *J. Appl. Electrochem.*, 2011, **41**, 363–375.

2 S. Singh and H. R. and Ghatak, *J. Wood Chem. Technol.*, 2017, **37**, 407–422.

3 P. Cai, F. Hongxian, C. Shuo, Q. Jian, Z. Songmei and L. Gang, *Electrochim. Acta*, 2018, **264**, 128–139.

4 M. Zirbes, D. Schmitt, N. Beiser, D. Pitton, T. Hoffmann and S. R. Waldvogel, *ChemElectroChem*, 2019, **6**, 155–161.

5 M. Zirbes, T. Graßl, R. Neuber and S. R. Waldvogel, *Angewandte Chemie International Edition*, 2023, **62**, e202219217.

6 N. D. Fidio, J. W. Timmermans, C. Antonetti, A. M. R. Galletti, R. J. A. Gosselink, R. J. M. Bisselink and T. M. Slaghek, *New J. Chem.*, 2021, **45**, 9647–9657.

7 Z. Fang, F. Li, M. Wang, F. Li, X. Wu, K. Fan, Q. Tang, L. Sun and P. Zhang, *Applied Catalysis B: Environmental*, 2023, **323**, 122149.

8 D. Gao, D. Ouyang and X. Zhao, *Chem. Eng. J.*, 2024, **479**, 147874.

9 C. Chen, Z. Zhou, J. Liu, B. Zhu, H. Hu, Y. Yang, G. Chen, M. Gao and J. Zhang, *Appl. Catal. B*, 2022, **307**, 121209.

10 Z. Wang, H. Du, Z. Liu, H. Wang, A. M. Asiri and X. Sun, *Nanoscale*, 2018, **10**, 2213–2217.

11 X. Yan, L. Tian, M. He and X. Chen, *Nano Lett.*, 2015, **15**, 6015–6021.

12 N. Bai, Q. Li, D. Mao, D. Li and H. Dong, *ACS Appl. Mater. Interfaces*, 2016, **8**, 29400–29407.

13 C. Wang, B. Tian, M. Wu and J. Wang, *ACS Appl. Mater. Interfaces*, 2017, **9**, 7084–7090.

14 H. Liu, X. Ma, Y. Rao, Y. Liu, J. Liu, L. Wang and M. Wu, *ACS Appl. Mater. Interfaces*, 2018, **10**, 10890–10897.

15 S. Fiameni, I. Herraiz-Cardona, M. Musiani, V. Pérez-Herranz, L. Vázquez-Gómez and E. Verlato, *Int. J. Hydrogen Energy*, 2012, **37**, 10507–10516.

16 F. Liu, W. He, Y. Li, F. Wang, J. Zhang, X. Xu, Y. Xue, C. Tang, H. Liu and J.

Zhang, *Appl. Surf. Sci.*, 2021, **546**, 149101.

17 W. Xie, K. Liu, G. Shi, X. Fu, X. Chen, Z. Fan, M. Liu, M. Yuan and M. Wang, *J. Energy Chem.*, 2021, **60**, 272–278.

18 F. Liu, F. Wang, X. Sun, Y. Wang, Y. Liu, S. Zhang, Y. Li, Y. Xue, J. Zhang and C. Tang, *Int. J. Hydrogen Energy*, 2024, **58**, 941–947.